Delivery of Peptide Coacervates to Form Stable Interaction Hubs in Cells

Wangjie Tu[1], Rachel Q. Theisen[2], Pengfei Jin[3], David M. Chenoweth[3,4], Amish J. Patel[5], Matthew C. Good[1,2,6*]

[1] Bioengineering Graduate Group, University of Pennsylvania, PA 19104

[2] Department of Cell and Developmental Biology, University of Pennsylvania, PA 19104

[3] Chemistry Graduate Group, University of Pennsylvania, PA 19104

[4] Department of Chemistry, University of Pennsylvania, PA 19104

[5] Chemical and Biomolecular Engineering Department, University of Pennsylvania, PA 19104

[6] Department of Bioengineering, University of Pennsylvania, PA 19104

* Correspondence: mattgood@pennmedicine.upenn.edu

Abstract

Cells contain membrane-bound and membraneless organelles that operate as spatially distinct biochemical niches. However, these subcellular reaction centers lose fidelity with aging and as a result of disease. A grand challenge for biomedicine is restoring or augmenting cellular functionalities. Although commonly tackled by gene replacement therapy, an excited new strategy is the delivery of protein-based materials that can directly interact with and alter biological networks inside a cell. In this study we sought to develop long-lasting materials capable of cellular uptake and incorporation, akin to an artificial organelle or intracellular interaction hub. Drawing inspiration from protein-based membranelles organelles, we developed a new delivery method to transplant micron size peptide-based compartments into living cells. We determined conditions to form large stable coacervates that are efficiently taken up by a variety of useful cell types and demonstrate their intracellular stability over time. We developed tools to enhance the extent and

spatial organization of cargo loading into these coacervates, including co-assembly of nanobodies that selectively bind to targets of interest. Combining them together, we demonstrate successful targeting of GFP protein inside cells. These results represent an important first step toward the development of deliverable synthetic organelles that can be fabricated in vitro and taken up by cells for applications in cell engineering and regenerative medicine.

Keywords

Synthetic hubs, designer organelles, coacervate delivery, disordered peptide, mesoscale intracellular compartment

Introduction

A grand challenge for biomedical science is achieving predictable control over cellular functions by controlling protein networks inside cells[1–3]. In nature, cells utilize spatial partitioning via anchoring and scaffold proteins and leverage subcellular compartmentalization as key strategies to enhance the efficiency of biochemical processes[4–6]. We previously demonstrated the feasibility of controlling cellular processes and cell behavior by expressing proteins capable of forming synthetic membraneless organelles intracellularly and targeting endogenous enzymes[7,8]. However, to date this approach has required gene delivery using viruses or nanoparticles. A major advance would be the ability to fabricate compartments ex vivo and deliver them into cells to stably function as designer synthetic hubs or organelles.

Cells control the rate and fidelity of biochemical reactions by compartmentalizing components in membrane-bound and membraneless organelles. For example, oxidative phosphorylation is caried out in lipid bilayer containing mitochondria[9], and membraneless organelles such as the nucleolus specifically govern rRNA processing[10–12]. Stress granules sequester factors to downregulate protein translation[13] and Nck-N-WASP condensates[14,15] recruit Sos1 and Arp2/3 to to form a reaction hub[16]. Membraneless compartments are formed by the self-assembly of proteins and RNAs intro micron-size condensates driven via multivalent interactions[6,17,18]. Similar ideology can be adopted to generate new designer condensates or compartments to programmably control reaction pathways in a cell[7,19,20]. Often the proteins that participate in this self-assembly and condensation contain large disordered or low-complexity polypeptide sequences[6,21]. We previously created synthetic condensates by expressing a disordered scaffold in cells and used them to reprogram cell behaviors. For example, we built compartments that functioned as insulators, turning signal flow on or off, to regulate growth and division or to polarize cytoskeleton organization[7]. Separately, synthetic condensates can be used as bioreactors to enhance signaling between components or generate new signaling cascades among factors that

normally only weakly interact[20,22]. However, there are limitations to the use of these approaches for clinical applications: gene delivery is required, gene expression has a maximum[23] that limits the amount of condensed material (expression relative to c_{sat})[8], and native targets must be tagged to drive their localization to the synthetic condensate[7,8]. We sought to overcome these hurdles using a novel strategy for protein-based delivery: peptide coacervates.

There are a variety of strategies to achieve protein or nucleic acid delivery to cells. Commonly the RNA for a target of interest is delivered via lipid nanoparticles, which then drives expression inside a cell[24]. However it is not feasible to achieve very high protein expression with these methods[23,25], which limits their utility for delivering materials to form protein condensates that function as synthetic organelles. Cell permeable peptides exist in nature and have been designed to be capable of crossing the plasma membrane[26–28]. Although useful for drug delivery, these short peptide sequences cannot simply be appended to target proteins of interest to drive their cellular uptake. Recently, a promising new strategy for protein delivery has emerged based on identification of peptide coacervate particles capable of crossing the plasma membrane for cellular uptake[29,30]. A novel 26 amino acid disordered peptide HBpep was identified and shown capable of self-assembly into micron size coacervates through liquid-liquid phase separation[29,31,32]. These particles readily cross the cell membrane for cytosolic delivery. With different variants, these coacervates can be co-assembled or loaded with cargos including proteins and RNAs and will partially disassemble upon entering the cells, highlighting their utility for efficiency cytosolic delivery of macromolecules[29,33,33,34]. Although primarily designed for drug delivery, we reasoned that the HBpep platform could be adapted to create stable protein-based hubs or organelles in cells, creating a new toolbox to augment or revitalize cellular functions.

In this study, we created a new platform to form large coacervates capable of uptake and stable maintenance inside living cells. We developed strategies to enhance protein cargo loading and

topological organization in coacervates, moving beyond passive loading and uniform partitioning. In contrast to previous controlled release systems, we developed strategies to deliver micron-size coacervates to cells that can serve as synthetic hubs or compartments, stable for days. Further we embedded nanobodies within these coacervates and demonstrated that they are capable of interfacing with protein targets in vitro and in cells. Delivery of synthetic hubs capable of targeting native enzymes and signaling pathways provides a powerful new strategy in cellular engineering. By eliminating the requirement to deliver genetic material, this modular platform promises to fast-track therapeutic development, for example through formation of degradomes or via compartments that rewire aberrant signaling responses.

Results

Parameter optimization to form stable micron-size protein coacervates

Building from a previous peptide coacervate platform, HBpep[31,33], we sought to develop a protocol to form gel-like particles that range in size from 1-5 μm diameter for cargo loading and cellular uptake, and that could ultimately serve as stable synthetic “hubs” or “organelles” in a cell. We chose to promote nucleation phase separation using two different methods: pH shift and temperature shift. HBpep contains five histidines and is largely soluble in acidic buffer, such as pH 4.5, but will phase separate at physiological pH 7.4 under standard conditions[35]. Further, HBpep displays upper critical solution temperature behavior and LLPS can be induced by shifting the temperature from 50°C to room temperature, 23°C. We also chose to test both the standard HBpep, which has only limited cargo release capability and a redox sensitive form HBpep-SA, that will release cargo into the cytoplasm of a cell[29].

We first measured coacervation via pH shift for HBpep and HBpep-SA over a range of peptide concentrations from 0.1 to 2 mg/mL, corresponding to approximately 35 – 700 micromolar. We found coacervate size and number depended on peptide concentration (**Fig. 1A-C**), as expected[36]. Although smaller particles have utility for drug delivery applications, we were interested in formation of larger hubs that would be stably maintained in cells. At concentrations of 0.5 mg/mL or higher, the average HBpep particle diameter was larger than 2 μm and could range from 1-6 μm (**Fig. 1B**). Similar results were attained with HBpep SA, although the sizes were slightly smaller. A higher fraction of the HBpep-SA peptide partitioned to the coacervates as measured by sedimentation of particles (**Fig. S1A-B**), although in both cases at majority of the scaffold peptide was condensed when assembled at a concentration of 0.5 mg/mL. We separately tested induction of LLPS via temperature shift and observed similar size and numbers of particles compared to induction via pH shift (**Fig. S1C-E**). During protocol optimization, we found that the free peptides in solutions at pH 7.4 were actually quite sticky and would foul surfaces of test tubes or imaging chambers over time. Particle production via pH shift is somewhat more reliable at creating dose-dependent coacervation and indicates use of acidic buffers for storage and handling of HBpep and HBpep-SA prior to assembly.

For coacervates to be useful for non-genetic delivery of 'hubs' to cells, they need to show gel-like material properties and not require free peptide present in the continuous phase to maintain their assembly. In contrast, liquid-like condensates of disordered proteins formed inside cells from gene expression can have high turnover because the protein is continuously expressed and maintained by a pool of material in the cytosol[37]. We thus tested the extent to which coacervates were in a gel-like or more liquid-like state by measuring labeled peptide diffusion following fluorescence recovery after photobleaching (FRAP). Particles were co-assembled with tracer amounts of a FITC-labeled HBpep (FITC-HBpep) (**Fig. S1F**) peptides and bleached using a 405 nm laser. Fluorescence recovery was very limited over time, for both types of peptides, indicating very slow

diffusion and suggesting that these particles are gels (**Fig. 1D,E**), as expected[34]. Recovery was slow both from full photobleaching of particles to measure recovery via diffusion from continuous phase, and when photobleaching a portion of the particle to measure diffusion inside the coacervate. We conclude it is feasible to generate particles of 1-5 μm in diameter using either method for to induce LLPS and that peptide concentration can be varied to tune average coacervate size. Given their gel-phase properties we expected it would be feasible to dilute them into new solutions without providing additional material in continuous phase and that they would remain stable.

Enhanced cargo loading into peptide coacervates via selective partitioning

We wondered whether it would be feasible to enhance selectivity and overall amount of cargo loaded into coacervates by tagging the cargo. Previous studies demonstrated non-specific entrapment or loading of cargos such as protein and RNA during assembly of HBpep and HBpep-SA coacervates[29]. However, loading efficiency varies for different cargos and depends on HBpep peptide concentration[29]. In this study, we explored increasing the specificity of cargo loading without having to adapt the cargo or change HBpep peptide concentration. We used GFP as a model folded protein cargo for this proof-of-concept test. To promote selective loading, we added a 25-amino-acid motif from HBpep (lacking tryptophan): GHGVY GHGVY GHGPY GHGPY GHGLY to the C-terminus of GFP, which we term GFP-HBP (**Fig. 2A**), and we generated the protein via recombinant expression and purification. We co-assembled the cargo via LLPS of HBpep and measured extent of loading. We compared loading of GFP vs GFP-HBP both for HBpep and HBpep-SA particles, in which particles were formed by pH shift. We found that HBpep enhanced cargo loading into coacervates (**Fig. 2B-D**), without changing coacervate sizes. We observed a nearly 2- to 3-fold increase in internal concentration of cargo as measured by fluorescence microscopy (**Fig. 2C, D**) and total partitioning as measured via sedimentation (**Fig. S2A, B**). We conclude it is feasible to enhance the overall magnitude of loading and internal

concentration of cargo by fusion of an HBP tag to a protein of interest. Under conditions in which cargos would compete, tagging would provide enhanced selectivity.

We next wondered whether it would be feasible to control the topology of cargo loading, dictating its spatial partitioning in the coacervate. Cargo loading appears relatively spatially uniform for coacervates formed via pH shift method, and in general cargos reach a higher internal concentration in particles comparing LLPS of HBpep via pH versus temperature for HBpep (**Fig. 2B**). Tagging greatly increases the partitioning of GFP to particles formed via temperature shift (**Fig. 2C**). Interestingly, the HBP tag also dictates the topology of cargo partitioning. GFP alone as a cargo shows relatively spatial uniform partitioning within particles, whereas GFP-HBP enriches at the particle surface (**Fig. 2B, C**). We conclude it is possible to specify a core-shell organization of scaffold and cargo that would enable spatially partitioning discrete cargos and would be broadly useful for a variety of applications in drug delivery and cell engineering. Nonetheless, for the remainder of this study we utilize pH shift to generate particles with uniform loading.

Delivering micron size or larger coacervates to cells and characterizing their stability

A previous study focused on delivery of particles smaller than 1 μm to cells and for the purpose of cytosolic particle dissociation and cargo release[29]. However, in this study, we were interested in using the HBpep and HBpep-SA platforms as stable synthetic hubs or organelles inside cells. As a result, we wanted to test the feasibility of delivering larger condensates to cells and their stability following uptake inside cells.

We sought to identify conditions to for highly efficient uptake of large particles in a variety of cell types. This included a transformed human cell line for osteosarcoma, U2OS, a mouse melanoma cell line, B16-F10, and primary human immune cells - monocytes (**Fig. 3A**). We pre-assembled

particles at 0.5 mg/mL, diluted them in cell media from 1:10 to 1:3 and measured particle uptake after 4 hrs and 24 hrs. Cells were washed extensively after particle addition to remove those not delivered to cells. We observed generally highly efficient uptake by cells for both particles of HBpep and HBpep-SA, in a variety of cell types (**Fig. 3A**). These particles were present in the cytosol, but not the nucleus (**Fig. 3A**) and showed diffusive motion (***Supp Movie1***). At 1 day, we measured effective and robust uptake of particles formed at both 0.2 and 2 mg/mL, averaging uptake of nearly 40 particles per cell at higher concentrations (**Fig. 3B-E**). Particle formulations include a range of sizes although those formed at 0.2 mg/mL, the mode for the distribution of diameters was less than 1 μm and those formed at 2 mg/mL were generally larger than 1 μm. Importantly there was a long tail in the distribution of particle sizes at higher concentrations (2 mg/mL formulation), and cells given these formulations contained nearly 10-fold higher numbers of larger particles, greater than 2 μm diameter (**Fig. 3D, E**). In exemplary cases we found it possible to fill up the cytoplasm of a cell with approximately 100 particles (**Fig. S3E, *Supp Movie 2***), a feat not possible from genetic expression of a coacervating protein. Therefore, it is feasible for larger coacervates to be efficiently taken up by cells.

In an effort to build stable hubs than can be delivered to cells, we were interested in the stability of the particles inside cells over time. Previous efforts focused on use of particles < 1 μm diameter for drug delivery that would subsequently partially disassemble in the cytoplasm[29]. We sought to test the stability of the intracellular coacervates, comparing formulations better suited for drug delivery versus those ideal for making stable hubs (**Fig. S3A-B**). Particles were generally more stable at day 5 for coacervates assembled at 2 mg/mL vs. 0.2 mg/mL, likely related to their larger sizes (**Fig. 3B, D and S3C**). Indeed, if when we quantified only larger particles (those > 2 μm diameter), the number per cell was relatively constant over time (**Fig. 3E**). In contrast smaller particles (< 2 μm diameter) were lost from cells for the 0.2 mg/mL formulation. A recent study suggests these coacervates cross the cell membrane via micropinocytosis which enables the

uptake of large portions of extracellular material[32]. We conclude that cells our large coacervates are efficiently taken up by cells, and that these particles are stable intracellularly for at least 5 days. These results provide a roadmap toward delivery and maintenance of synthetic 'hubs' within living cells without the need for gene transfer.

Selective targeting of proteins to pre-formed coacervates using nanobodies in vitro

To be useful as a designer organelle or hub, coacervates must be functionalized with molecules that enable them to interface with native protein interaction networks or signaling pathways. Native membraneless organelles can function as insulators[13] – sequestering components – or as bioreactor compartments that co-localize components at elevated concentrations[15]. We previously demonstrated that synthetic condensates could be formed via expression of a scaffold protein in cells, and that they could function as insulators, targeting and partitioning native enzymes that were tagged with a complementary coiled coil[7]. In this study we wanted to go further: to deliver synthetic hubs via extracellular uptake rather than via gene transfer and expression, and to embed nanobodies within them that could bind to a target of interest without needing to tag the target. It would then be possible to create a designer biochemical niche inside a cell through the delivery of a one-pot peptide coacervate platform.

To start, we tested the feasibility of targeting proteins to the peptide coacervates in vitro comparing those containing or lacking a nanobody (**Fig. 4A**). As a proof-of-concept we tested co-assembly and embedding of the nanobody VHH4 which binds with nanomolar affinity to GFP[38]. This nanobody is highly useful because many stable cell lines have been created that contain a GFP-fusion to a target protein of interest. To track nanobody loading using fluorescence microscopy we fused it to mCherry (VHH4-mCherry), or also to the HBP targeting sequence (VHH4-mCherry-HBP). To form particles, these purified proteins were added a 1:5 mass ratio into formulations of 0.5mg/mL HBpep and HBpep-SA. Both nanobody cargos enriched within the HBpep and HBpep-

SA particles after co-assembly (**Fig. 4B and S4A, C**). We also observed somewhat elevated loading of VHH4-mCherry-HBP into HBpep particles (**Fig. S4A, C**), consistent with the results described in Figure 2.

Once particles were formed, we measured partitioning of GFP target protein added to pre-formed coacervates in an imaging microwell. Particles lacking a VHH4 nanobody did not enrich GFP and instead partially excluded it (**Fig. 4B, C**); note partition coefficient of less than 1. Thus, cargo uptake is almost non-existent following peptide coacervate formation. In contrast particles containing VHH4 nanobody enriched the GFP target at their interface (**Fig. 4B**) and this enrichment or partition coefficient at the surface was approximately 2-to 4- fold (**Fig. 4C, S4D**) dependent on the type of peptide and whether HBP was present or not on the nanobody. Note that the nanobody loading is relatively uniform throughout particles, and thus the surface targeting is not caused by spatial partitioning of nanobody to periphery. It was recently shown that these gel-like particles of HBpep and HBpep-SA have limited permeability for macromolecules larger than 2-10 kDA[39]. At 27 kDa in molecular weight, the target GFP would be expected to have limited diffusion inside the coacervate in the time course of our experiments, consistent with the ring-like GFP partitioning to our VHH4 containing coacervates (**Fig. 4B, S4B**)

Although mostly surface recruitment was achieved for this in vitro test using VHH4 and GFP, it should be possible to achieve higher internal partitioning of molecules with smaller molecular weights or by allowing cargos to incubate with coacervates for longer periods of time. Notably for drug delivery, the cargo can be co-assembled with the particle as we show in Figure 2. To conclude, in this initial test we sought and found proof of feasibility for selective binding of target proteins to coacervates using nanobodies. Next, we wanted to test these particles for targeting in living cells.

Target enrichment at synthetic protein hubs inside cells

It has been suggested that HBpep particles are taken up by cells through actin-mediated macropinocytosis and phagocytosis[32]. In such a process, the coacervates will be encapsulated by lipid membrane, which poses a potential challenge for binding of target protein proteins. Based on published results and our own GFP delivery experiments using HBpep-SA particles (**Fig. S3D**), some GFP can be released into the cytosol, which implies that there may be some stochastic escape from membrane encapsulation. However to further promote endosomal escape, we included TAT-HA2 assist peptide[40] in co-assembly of HBpep-SA particles loaded with VHH4 nanobody or a control protein. As a test case, we used a U2OS human cell line that was virally transduced to stably expressed GFP as a target protein.

To determine whether coacervates could function as hubs in cells we wanted to compare target GFP binding to control mCherry containing HBpep-SA particles versus those containing the VHH4-mCherry nanobody. In cells loaded with control particles, we observed that most coacervates excluded the target GFP (**Fig. 5A, C**), showing a partition coefficient less than 1. In contrast for VHH4-mCherry group, although many coacervates did not sequester the target (likely due to presence of membrane), we saw a large significant jump in target binding (**Fig. 5B, D**). The partition coefficients achieved both for scaffold and target are on par with our previous study which used coiled-coil recruitment of targets into RGG condensates[7]. In cells, enrichment indices below 2 are often non-specific. For control mCherry particles target GFP enrichment was below this value in nearly every case; we observed it < 1% of time (**Fig. 5E**). In contrast hubs containing VHH4-mCherry and TAT-HA2 assist peptide showed target GFP partitioning as high as 15-fold above cytosolic levels (**Fig. 5D, S5A**). The percentage of condensates with GFP enrichment > 2 was approximately 11.5% for particles co-assembled with VHH4-mCherry and TAT-HA2, representing an order of magnitude increase in target enrichment compared to control particles. There is also a general trend of increasing average GFP enrichment among condensates with

GFP enrichment > 1 with VHH4-mCherry and TAT-HA2 loaded compared to control group (**Fig. S5B**).

A somewhat surprising result from the in vivo experiment is the topology of target recruitment. In our in vitro experiments (Fig 4), VHH4-mCherry loaded condensates were only able to recruit GFP to the surface, likely limited by the small coacervate pore size[39]. However, once HBpep-SA condensates are taken up by cells, we observe target GFP recruitment to the hub interior (**Fig. 5B, D**). This difference of recruitment topology between in vitro and in vivo experiment may imply that HBpep-SA condensates are partially disassembled in cytosol, which increases the pore sizes and allow larger molecules such as GFP to diffuse in, although more testing is needed.

We conclude it is feasible to deliver nanobody coacervates to cells that can function for days as stable hubs, capable of targeting endogenously expressed proteins to the microcompartment. Limitations of the current study include only partial endosomal release, which requires further optimization. These results demonstrate a path toward remodeling protein interaction networks in living cells using synthetic hubs or organelles and represent a unique opportunity for cell engineering without the requirement for gene delivery.

Materials and Methods

Peptides and Coacervate Formation

HBpep and FITC-HBpep peptides were customize ordered from Genescript

HBpep-SA peptides (HY-000) were ordered from MCE (MedChemExpress)

HBpep amino acid sequence[29]: GHGVY GHGVY GHGPY GHGPY GHGLY W

Temperature shift method to induce LLPS

In this method, HBpep peptide powder were dissolved in 1xPBS buffer at pH7.4, aliquoted as a high concentration stock and stored in -80C. To make condensates, HBpep peptide and cargo are added to 1x PBS and mixed, with all reagents in a bead bath at 50°C. Following 10 mins of incubation, the tube is shifted back to room temperature (~23°C) for 15mins.

pH shift method to induce LLPS

In this method, HBpep and HBpep-SA peptide powder were dissolved in 50mM acetate buffer at pH 4.5, aliquoted as a high concentration stock and stored in -80°C. To make condensates HBpep or HBpep-SA peptides were added sequentially to a solution of water, salt and cargo. After thorough mixing, 10x phosphate buffer was added to shift the pH to ~7.4. We waited 15 minutes at room temperature for coacervate particle formation and gelation after the pH shift.

Delivery of condensates to cells

Cells were seeded at 50% confluency one day before delivery in glass bottom 96-well plates (Cellvis P96-1-N). At this time, a final concentration of 10μg/mL DAPI was added in the culture to stain nucleus. On the day of condensate delivery, cells were first washed with growth medium: DMEM for B16-F10 melanoma cells and EMEM for U2OS cells. For condensate delivery, growth medium was replaced by Opti-MEM and condensates in a volume of between 10-30 μl were added to Opti-mem for a final volume of 100 μl of. Particle uptake was detectable within 4 hr and cells were generally quantified at 24 hr after coacervate addition. Membranes were stained by Abcam Cytopainter Cell Membrane Staining Kit in the experiment in Figure3A. For stability test in Figure 3B-E, U2OS cells were cultured in EMEM for 5 days.

Protein purification

Tag-free GFP was purchased from abcam (ab84191, Recombinant A. victoria GFP protein). Codon-optimized 6his-GFPHBP, 6his-mCherry, 6his-VHH4-mCherry, 6his-VHH4-mCherry-HBP constructs were cloned into pET expression vectors, by In-Fusion ligation (Takara Bio) and transformed into Rosetta 2 Escherichia coli cells (Sigma Aldrich). Bacterial cultures were grown in Luria broth supplemented with kanamycin and chloramphenicol at 37 °C to an OD600 of 0.6–0.8, and expression was induced by 0.5 mM isopropyl β-D-1-thiogalactopyranoside at 16 °C overnight (18hr). Cell cultures were centrifuged at 1,960g in a Sorvall RC6+ centrifuge (Thermo Scientific), and the resulting pellets were collected and stored at −80 °C. Bacterial pellets were thawed, then resuspended in lysis buffer (50 mM Tris-HCl, pH 7.5, 1 M NaCl, 20 mM imidazole, 1 mM β-mercaptoethanol) and complete EDTA-free protease inhibitor cocktail (Roche). Cells were lysed with 2 minutes of sonication at 50% power using a Branson Sonifier. Lysates were clarified by centrifugation at 13,250g for 20 min in a Sorvall RC6+ centrifuge using a F21S-8x50y rotor (Thermo Fisher Scientific) at 4 °C. The supernatant of lysate were incubated with Ni–NTA beads (Thermo Fisher Scientific) while rotating at for 4 °C 1 h. Beads were then washed three times. Proteins were eluted by lysis buffer containing 500 mM imidazole and 1 mM dithiothreitol (DTT). Eluted proteins were dialyzed overnight into PBS buffer (10mM Na2HPO4,1.8mM KH2PO4, 2.7mM KCL, 137 mM NaCl, pH7.4) using a Slide-A-Lyzer membrane cassette (Thermo Fisher Scientific) with a 10-kDa size cutoff at room temperature[41].

Mammalian cell procedures

U2OS cells were cultured in Eagle's minimal essential medium (EMEM, Quality Biological) supplemented with 10% fetal bovine serum (Gibco), 2 mM L-glutamine (Gibco) and 10 U mL−1 penicillin-streptomycin (Gibco). B16 cells were cultured in Dulbecco's Modified Eagle's Medium supplemented with 10% fetal bovine serum (Gibco), 2 mM L-glutamine (Gibco) and 10 U mL−1 penicillin-streptomycin (Gibco). Cells are maintained at 37 °C in a humidified atmosphere with 5% CO2. Cells were split in 1:5 ratio every three days and had been passaged for less than two

months, were negative for known infection. Frozen human primary monocytes were obtained from Penn Human Immunology Core, then thawed and cultured in RPMI1640 with 10% fetal bovine serum (Gibco), 2 mM L-glutamine (Gibco) and 10 U mL−1 penicillin-streptomycin (Gibco).

Microscopy

Images were collected on an Olympus IX81 inverted confocal microscope (Olympus Life Science) equipped with a Yokogawa CSU-X1 spinning disk, a mercury lamp, 405- 488- and 561-nm laser launches, and an iXon3 electron-multiplying charge-coupled device (EMCCD) camera (Andor). Multidimensional acquisition was controlled by MetaMorph software (Molecular Devices, version 7.8.10.0). Samples were illuminated using a 405-nm laser and/or 488-nm laser and/or a 561-nm laser and were imaged through a ×100, 1.4-NA oil immersion objective and/or a x20, 0.75NA air objective. Z stacks were collected in 0.3-μm steps.

For in vitro experiments, HBpep and HBpep-SA condensates were imaged in custom-fabricated acrylic gasket chambers adhered to glass coverslips (#1.5 glass thickness; Corning Inc.) The glass bottom was passivated by 10mg/mL BSA overnight. For in vivo experiments, cells were seeded in glass bottom 96-well plates (Cellvis P96-1-N).

For FRAP experiments on FITC-HBpep labeled HBpep and HBpep-SA condensates, a Roper iLas2 photoactivation system controlling a 405-nm laser was used. An area containing multiple condensates were selected and photobleached, and fluorescence recovery in the bleached region was analyzed in ImageJ after normalizing the fluorescence intensity from 0 to 100 based on the florescence intensity before FRAP and right after FRAP. Images were collected to visualize the condensates at the 488-nm wavelength and bright field using a ×100, 1.4-NA oil immersion objective.

Image analysis

Image segmentation and analysis were performed in FIJI and Excel. “Analyze Particle” function in FIJI was used to count and measure the size of condensates in Figure1 and FigureS1 and measure the average fluorescence intensity in condensates in Figure2, except the GFP loading in HBpep through temperature group. In other quantifications, measure of condensate size, number and fluoresce intensity were measured manually in FIJI. Enrichment Index in Figure2 about GFP and GFPHBP loading was calculated by mean fluorescence intensity of whole condensates divided by average fluorescence intensity in the liquid phase outside condensates. In Figure4, a line scan was first done in FIJI over the condensate on 488nm channel. Then, the maximum fluorescence intensity was recorded and divided by the average fluorescence intensity in the liquid phase outside condensates to get the ring enrichment index. In Figure5 and FigureS5, a line scan was first done in FIJI over the condensate in 488 nm channel. Then, the maximum fluorescence intensity was recorded and divided by the average fluorescence intensity in the cell cytosol to get the maximum enrichment index. The 3D reconstruction in the Supplement Movie2 was rendered in Imaris.

Statistics and reproducibility

The experiments were reproducible. All statistical analyses were performed in GraphPad Prism 9. To test the significance of two categories, an unpaired one-tailed Welch’s t-test was used. To test the significance of more than two categories, a one-way Brown-Forsythe ANOVA was used. In all cases, NS indicates not significant ($P > 0.05$), *$P \leq 0.05$, **$P \leq 0.01$, ***$P \leq 0.001$ and ****$P \leq 0.0001$.

Acknowledgements

We thank A. Stout and the Penn CDB Microscopy Core for imaging support, Penn Human Immunology Core for human primary monocytes, and M. Wadley for human primary monocytes cell culture. This study was partially supported by the National Institute of Biomedical Imaging and Bioengineering grant, EB028320 (M.C.G.), by National Science Foundation through the University of Pennsylvania Materials Research Science and Engineering Center (MRSEC) (DMR-2309043), and a seed award from the Center for Precision Engineering for Health (CPE4H) at the University of Pennsylvania (M.C.G., A.J.P.)

Author Contributions.

M.C.G, W.T. and A.J.P. conceptualized the project. M.C.G., W.T. R.Q.T., D.M.C. designed the experiments. W.T. and P.J. performed initial peptide synthesis. W.T. and R.Q.T. designed and cloned genetic constructs. W.T. purified cargo and nanobody proteins and performed experiments for assembly, co-assembly, FRAP, in vitro targeting experiments and coacervate stability experiments. W.T. and R.Q.T performed imaging for characterization of coacervate distribution and mobility in various cell types. W.T. performed experiments for GFP targeting in cells. W.T. analyzed experimental data. M.C.G and W.T. wrote the manuscript with feedback from A.J.P. and D.M.C.

Competing Interests.

The authors declare no competing interests.

Materials and Correspondence

Plasmids will be made available on Addgene and upon request to Prof. Matthew Good: mattgood@pennmedicine.upenn.edu

Bibliography

1. Sadelain, M., Rivière, I. & Riddell, S. Therapeutic T cell engineering. *Nature* **545**, 423–431 (2017).
2. Lim, W. A. & June, C. H. The Principles of Engineering Immune Cells to Treat Cancer. *Cell* **168**, 724–740 (2017).
3. Chen, Z. & Elowitz, M. B. Programmable protein circuit design. *Cell* **184**, 2284–2301 (2021).
4. Pawson, T. & Scott, J. D. Signaling Through Scaffold, Anchoring, and Adaptor Proteins. *Science* **278**, 2075–2080 (1997).
5. Good, M. C., Zalatan, J. G. & Lim, W. A. Scaffold Proteins: Hubs for Controlling the Flow of Cellular Information. *Science* **332**, 680–686 (2011).
6. Banani, S. F., Lee, H. O., Hyman, A. A. & Rosen, M. K. Biomolecular condensates: organizers of cellular biochemistry. *Nat Rev Mol Cell Biol* **18**, 285–298 (2017).
7. Garabedian, M. V. *et al.* Designer Membraneless Organelles Sequester Native Factors for Control of Cell Behavior. *Nat Chem Biol* **17**, 998–1007 (2021).
8. Schuster, B. S. *et al.* Controllable protein phase separation and modular recruitment to form responsive membraneless organelles. *Nat Commun* **9**, 2985 (2018).
9. McBride, H. M., Neuspiel, M. & Wasiak, S. Mitochondria: More Than Just a Powerhouse. *Current Biology* **16**, R551–R560 (2006).
10. Boulon, S., Westman, B. J., Hutten, S., Boisvert, F.-M. & Lamond, A. I. The Nucleolus under Stress. *Molecular Cell* **40**, 216–227 (2010).
11. Lafontaine, D. L. J., Riback, J. A., Bascetin, R. & Brangwynne, C. P. The nucleolus as a multiphase liquid condensate. *Nat Rev Mol Cell Biol* **22**, 165–182 (2021).
12. Mitrea, D. M. *et al.* Nucleophosmin integrates within the nucleolus via multi-modal interactions with proteins displaying R-rich linear motifs and rRNA. *eLife* **5**, e13571.

13. Protter, D. S. W. & Parker, R. Principles and Properties of Stress Granules. *Trends in Cell Biology* **26**, 668–679 (2016).

14. Li, P. *et al.* Phase Transitions in the Assembly of Multi-Valent Signaling Proteins. *Nature* **483**, 336–340 (2012).

15. Banjade, S. & Rosen, M. K. Phase transitions of multivalent proteins can promote clustering of membrane receptors. *eLife* **3**, e04123 (2014).

16. Huang, W. Y. C. *et al.* A molecular assembly phase transition and kinetic proofreading modulate Ras activation by SOS. *Science* **363**, 1098–1103 (2019).

17. Yoshizawa, T., Nozawa, R.-S., Jia, T. Z., Saio, T. & Mori, E. Biological phase separation: cell biology meets biophysics. *Biophys Rev* **12**, 519–539 (2020).

18. Langdon, E. M. & Gladfelter, A. S. A New Lens for RNA Localization: Liquid-Liquid Phase Separation. *Annual Review of Microbiology* **72**, 255–271 (2018).

19. Dzuricky, M., Rogers, B. A., Shahid, A., Cremer, P. S. & Chilkoti, A. De novo engineering of intracellular condensates using artificial disordered proteins. *Nat. Chem.* **12**, 814–825 (2020).

20. Sang, D. *et al.* Condensed-phase signaling can expand kinase specificity and respond to macromolecular crowding. *Molecular Cell* **82**, 3693-3711.e10 (2022).

21. Piovesan, D. *et al.* MobiDB: 10 years of intrinsically disordered proteins. *Nucleic Acids Research* **51**, D438–D444 (2023).

22. Zhao, E. M. *et al.* Light-based control of metabolic flux through assembly of synthetic organelles. *Nat Chem Biol* **15**, 589–597 (2019).

23. Dou, Y. *et al.* The CAG promoter maintains high-level transgene expression in HEK293 cells. *FEBS Open Bio* **11**, 95–104 (2021).

24. Mitchell, M. J. *et al.* Engineering precision nanoparticles for drug delivery. *Nat Rev Drug Discov* **20**, 101–124 (2021).

25. Müller, J. A. *et al.* Kinetics of RNA-LNP delivery and protein expression. *European Journal of Pharmaceutics and Biopharmaceutics* **197**, 114222 (2024).

26. Guidotti, G., Brambilla, L. & Rossi, D. Cell-Penetrating Peptides: From Basic Research to Clinics. *Trends in Pharmacological Sciences* **38**, 406–424 (2017).

27. Lindgren, M. *et al.* Cell-penetrating peptides. *Trends in Pharmacological Sciences* **21**, 99–103 (2000).

28. Koren, E. & Torchilin, V. P. Cell-penetrating peptides: breaking through to the other side. *Trends in Molecular Medicine* **18**, 385–393 (2012).

29. Sun, Y. *et al.* Phase-separating peptides for direct cytosolic delivery and redox-activated release of macromolecular therapeutics. *Nat. Chem.* **14**, 274–283 (2022).

30. Cao, S. *et al.* Dipeptide coacervates as artificial membraneless organelles for bioorthogonal catalysis. *Nat Commun* **15**, 39 (2024).

31. Lim, J. *et al.* Liquid–Liquid Phase Separation of Short Histidine- and Tyrosine-Rich Peptides: Sequence Specificity and Molecular Topology. *J. Phys. Chem. B* **125**, 6776–6790 (2021).

32. Shebanova, A. *et al.* Cellular Uptake of Phase-Separating Peptide Coacervates. *Advanced Science* **11**, 2402652 (2024).

33. Sun, Y. *et al.* Redox-Responsive Phase-Separating Peptide as a Universal Delivery Vehicle for CRISPR/Cas9 Genome Editing Machinery. *ACS Nano* **17**, 16597–16606 (2023).

34. Sun, Y. *et al.* Phase-separating peptide coacervates with programmable material properties for universal intracellular delivery of macromolecules. *Nat Commun* **15**, 10094 (2024).

35. Sun, Y. *et al.* Redox-Responsive Phase-Separating Peptide as a Universal Delivery Vehicle for CRISPR/Cas9 Genome Editing Machinery. *ACS Nano* **17**, 16597–16606 (2023).

36. Gudlur, S. *et al.* pH-dependent interactions of coacervate-forming histidine-rich peptide with model lipid membranes. *Front. Soft Matter* **3**, (2024).

37. Bentley, E. P., Frey, B. B. & Deniz, A. A. Physical Chemistry of Cellular Liquid-Phase Separation. *Chemistry – A European Journal* **25**, 5600–5610 (2019).

38. Kubala, M. H., Kovtun, O., Alexandrov, K. & Collins, B. M. Structural and thermodynamic analysis of the GFP:GFP-nanobody complex. *Protein Sci* **19**, 2389–2401 (2010).

39. Lim, J. *et al.* Hierarchical structural organization in bioinspired peptide coacervate microdroplets. *bioRxiv* (2024).

40. Wadia, J. S., Stan, R. V. & Dowdy, S. F. Transducible TAT-HA fusogenic peptide enhances escape of TAT-fusion proteins after lipid raft macropinocytosis. *Nat Med* **10**, 310–315 (2004).

41. Welles, R. M. *et al.* Determinants that enable disordered protein assembly into discrete condensed phases. *Nat. Chem.* **16**, 1062–1072 (2024).

Figure 1. Assembly and size control of HBpep and HBpep-SA gel-like peptide coacervates

(A) Images showing assembly of coacervate particles from HBpep and HBpep-SA using pH shift method at different concentrations of peptide. Solutions were at room temperature, 100 mM NaCl and at pH 7.4. Scale bar: 10 μm. **(B)** Quantification of HBpep and HBpep-SA coacervate diameters at different concentrations via pH shift method. The number of coacervates used for quantification per group, n=242, 620, 592, 172, 235, 678, 647 from left to right groups. **(C)** Quantification of average number of HBpep and HBpep-SA coacervates upon assembly at different concentrations (number per 4616.2 μm^2 imaging area). The number of 4616.2 μm^2 images used per group, n=3. Error bars indicate standard deviation. **(D)** Fluorescence images over time of FITC labeled (1:100) HBpep and HBpep-SA coacervates formed at 0.5 mg/mL via pH shift, following laser photobleaching. Scale bar: 5 μm. **(E)** Quantification of normalized fluorescence after FRAP, showing intensity within bleached region of FITC labeled HBpep and HBpep-SA coacervates formed via pH shift. Green line: HBpep whole condensate FRAP. Green dash line: HBpep-SA whole condensate FRAP. Blue line: HBpep-SA partial condensate FRAP.

Figure 2. Enhanced cargo loading and topological partitioning using disordered peptide tags

(A) Scheme showing strategy to enhance selectivity of cargo loading: comparing of GFP vs tagged GFP-HBP loaded in HBpep condensates through pH shift (left) or temperature shift (right) method. **(B)** Images of cargo loading into coacervates: 0.1 mg/mL GFP or GFP-HBP co-assembled (loaded) into 0.5mg/mL HBpep or HBpep-SA particles through pH or temperature shift. Scale bar: 10 μm. **(C)** Quantitation of cargo loading via normalized line scan, averaging GFP or GFPHBP in coacervates of similar size. n=5 from (B). **(D)** Quantification of fluorescence intensity of cargo loading for GFP and GFPHBP in HBpep or HBpep-SA coacervates. Enrichment index: fluorescence intensity in coacervate divided by the continuous phase. The number of coacervates used for quantification per group, n=68,150, 293, 228, 322, 322 from left to right groups. Error

bars indicate the standard deviation. NS indicates not significant ($P > 0.05$), *$P \leq 0.05$, **$P \leq 0.01$, ***$P \leq 0.001$ and ****$P \leq 0.0001$.

Figure 3. Stable delivery of peptide coacervates to mouse and human cells and clinically relevant cell types

(A) Fluorescence images of coacervate uptake in cell lines. 30ul of HBpep particles assembled at 1mg/mL or 30ul HBpep-SA particles assembled at 0.5mg/mL were added to the cell media for human osteosarcoma line U2OS, B16-F10 murine melanoma cells, and primary human monocytes. Green: FITC labeled condensates. Red: Abcam Cytopainter Cell Membrane Staining. Blue: Nucleus, stained DNA (DAPI). Scale bar: 10 μm. **(B)(D)** Quantification of size and number of coacervate taken up per cells; for formulations of 20 μl 0.2 mg/mL or 10ul 2 mg/mL HBpep-SA delivered to U2OS; following particles over the course of 5 days. For coacervate size quantification, n=255, 108, 19 for 0.2mg/mL from Day1 to Day5 and n= 364, 400, 353 for 2mg/mL from Day1 to Day5. For coacervate number per cell quantification, cell number n=10. Error bars indicate standard deviation. **(C)** Fluorescence images of U2OS cells with particles at day 1 and day 5. Scale bar: 10 μm. **(E)** Quantification of the number of large coacervates (diameter > 2 μm) per cell compared to smaller ones (diameter < 2 μm) for particles assembled at 2 mg/mL and 0.2 mg/mL HBpep-SA. The number of cells used for quantification per group, n=10. Error bars indicate the standard deviation. NS indicates not significant ($P > 0.05$), *$P \leq 0.05$, **$P \leq 0.01$, ***$P \leq 0.001$ and ****$P \leq 0.0001$.

Figure 4. Selective binding of protein targets to nanobody containing coacervates in vitro

(A) Scheme to determine selectivity of target binding to mCherry loaded or VHH4-mCherry loaded HBpep coacervates. VHH4 nanobody binds GFP. **(B)** Fluorescence images of cargo (mCherry or VHH4 mCherry) and target protein (GFP) added following addition of 1uM target protein. Images taken 5mins after GFP added. scale bar: 10 μm. **(C)** Quantification of the enrichment of target

GFP to HBpep-SA coacervates. enrichment index: intensity of fluorescence on particle surface division by surrounding solution. The number of condensates used for quantification per group: n=20. The error bars indicate standard deviation. NS indicates not significant ($P > 0.05$), *$P \leq 0.05$, **$P \leq 0.01$, ***$P \leq 0.001$ and ****$P \leq 0.0001$.

Figure 5. Delivered VHH4-HBpep-SA "Hubs" bind to and enrich native target GFP protein

(A)(B) Representative fluorescence images of target binding to hubs inside U2OS cells stably expressing GFP, comparing mCherry control and VHH4(nanobody)mCherry-loaded coacervates. 30ul of coacervates formed from 0.5 mg/mL HBpep-SA, co-assembled with 0.1mg/mL mCherry or VHH4-mCherry were added to the cell media for U2OS cells and imaged at 24 hr. Cell boundaries are indicated by dashed gray line. Chosen 'hub' for line scan is indicated by white line. Scale bar: 10 μm. **(C)(D)** Line scans of coacervate hubs showing fluorescence enrichment in (A)(B). **(E)** Quantification: percentage of hubs that show target enrichment greater than 2.

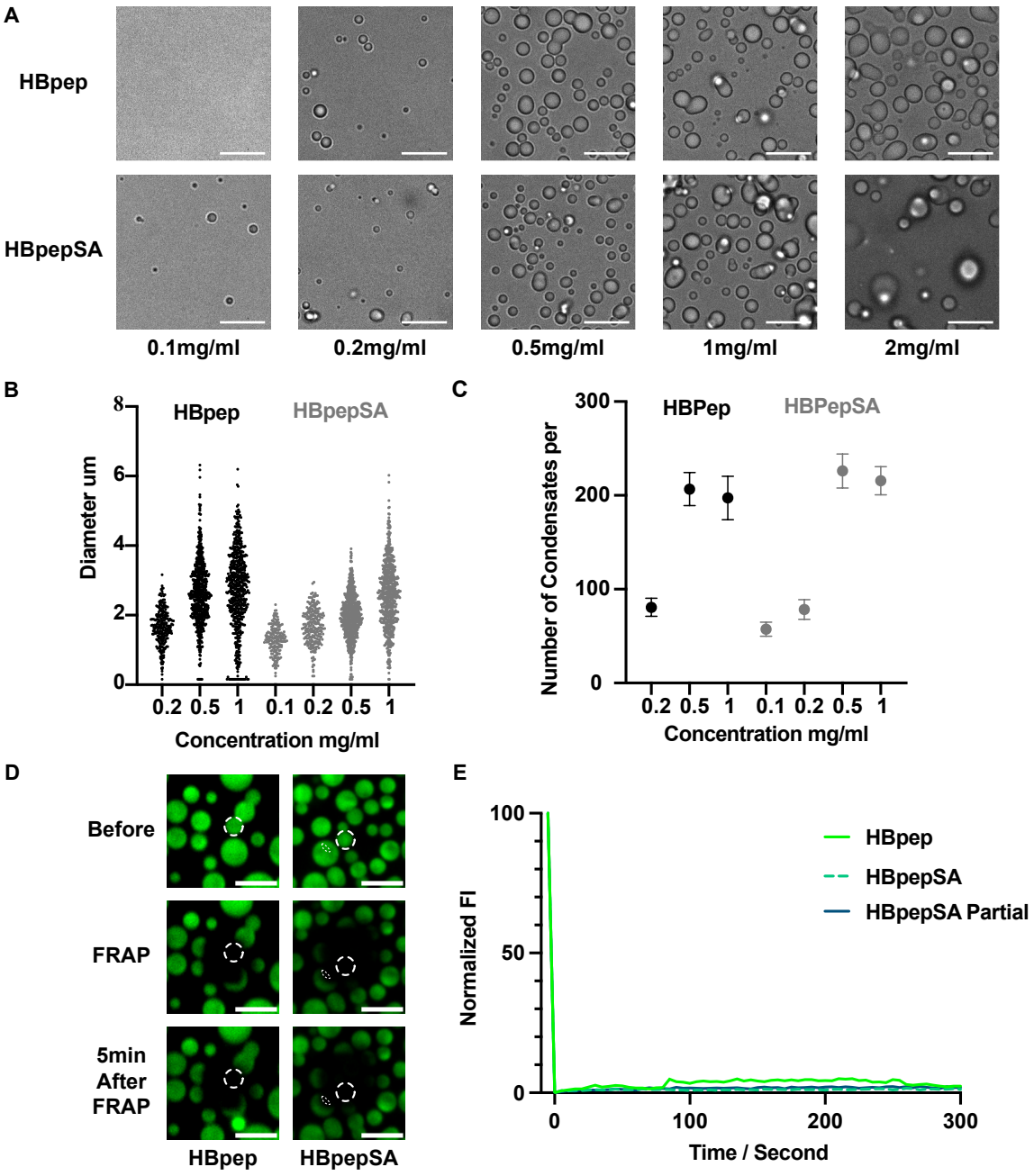

Figure 1. Assembly and size control of HBpep and HBpep-SA gel-like peptide coacervates
(A) Images showing assembly of coacervate particles from HBpep and HBpep-SA using pH shift method at different concentrations of peptide. Solutions were at room temperature, 100 mM NaCl and at pH 7.4. Scale bar: 10 µm. **(B)** Quantification of HBpep and HBpep-SA coacervate diameters at different concentrations via pH shift method. The number of coacervates used for quantification per group, n=242, 620, 592, 172, 235, 678, 647 from left to right groups. **(C)** Quantification of average number of HBpep and HBpep-SA coacervates upon assembly at different concentrations (number per 4616.2 μm^2 imaging area). The number of 4616.2 μm^2 images used per group, n=3. Error bars indicate standard deviation. **(D)** Fluorescence images over time of FITC labeled (1:100) HBpep and HBpep-SA coacervates formed at 0.5 mg/mL via pH shift, following laser photobleaching. Scale bar: 5 µm. **(E)** Quantification of normalized fluorescence after FRAP, showing intensity within bleached region of FITC labeled HBpep and HBpep-SA coacervates formed via pH shift. Green line: HBpep whole condensate FRAP. Green dash line: HBpep-SA whole condensate FRAP. Blue line: HBpep-SA partial condensate FRAP.

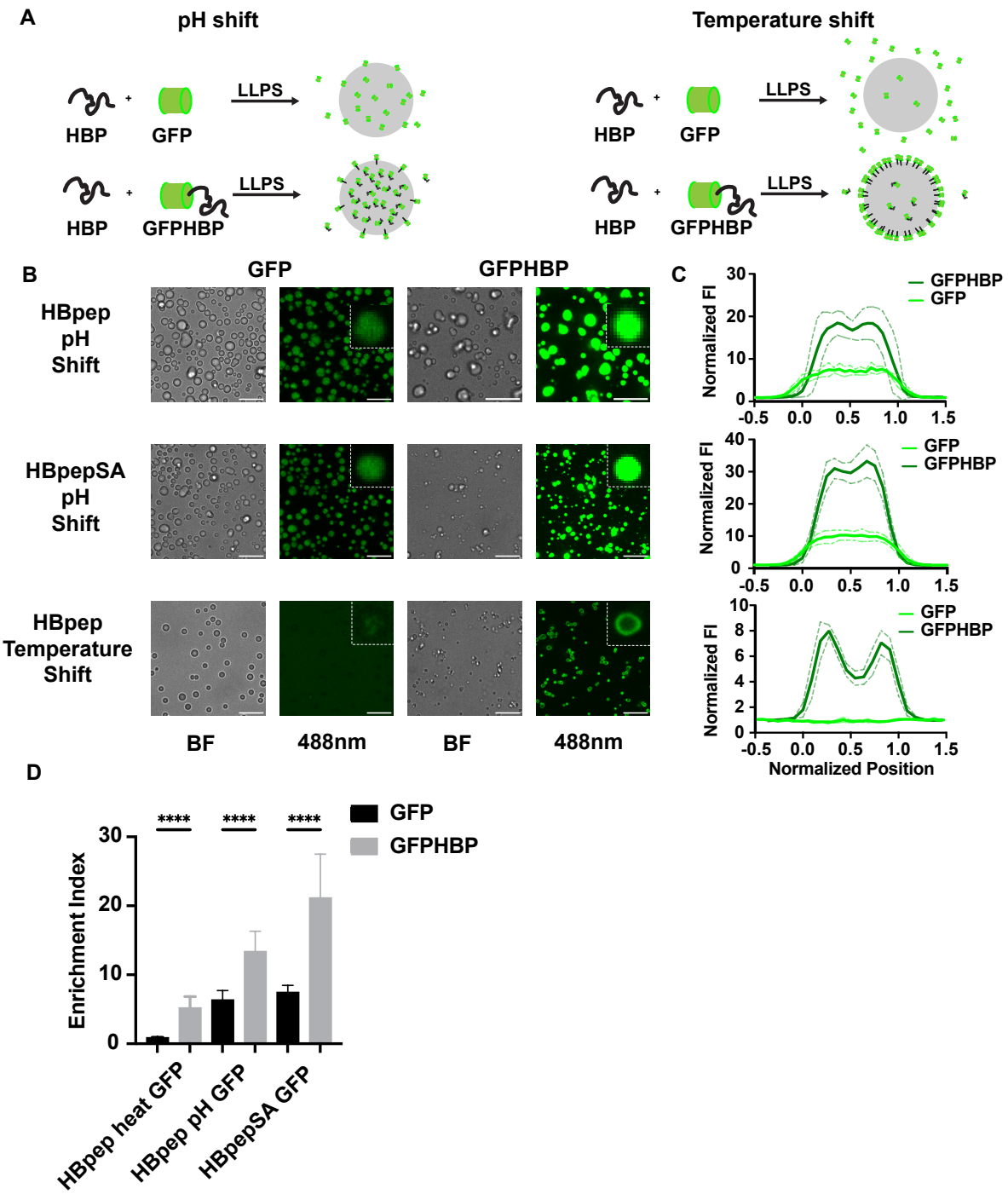

Figure 2. Enhanced cargo loading and topological partitioning using disordered peptide tags
(A) Scheme showing strategy to enhance selectivity of cargo loading: comparing of GFP vs tagged GFP-HBP loaded in HBpep condensates through pH shift (left) or temperature shift (right) method. **(B)** Images of cargo loading into coacervates: 0.1 mg/mL GFP or GFP-HBP co-assembled (loaded) into 0.5mg/mL HBpep or HBpep-SA particles through pH or temperature shift. Scale bar: 10 µm. **(C)** Quantitation of cargo loading via normalized line scan, averaging GFP or GFPHBP in coacervates of similar size. n=5 from (B). **(D)** Quantification of fluorescence intensity of cargo loading for GFP and GFPHBP in HBpep or HBpep-SA coacervates. Enrichment index: fluorescence intensity in coacervate divided by the continuous phase. The number of coacervates used for quantification per group, n=68,150, 293, 228, 322, 322 from left to right groups. Error bars indicate the standard deviation. NS indicates not significant ($P > 0.05$), *$P \leq 0.05$, **$P \leq 0.01$, ***$P \leq 0.001$ and ****$P \leq 0.0001$.

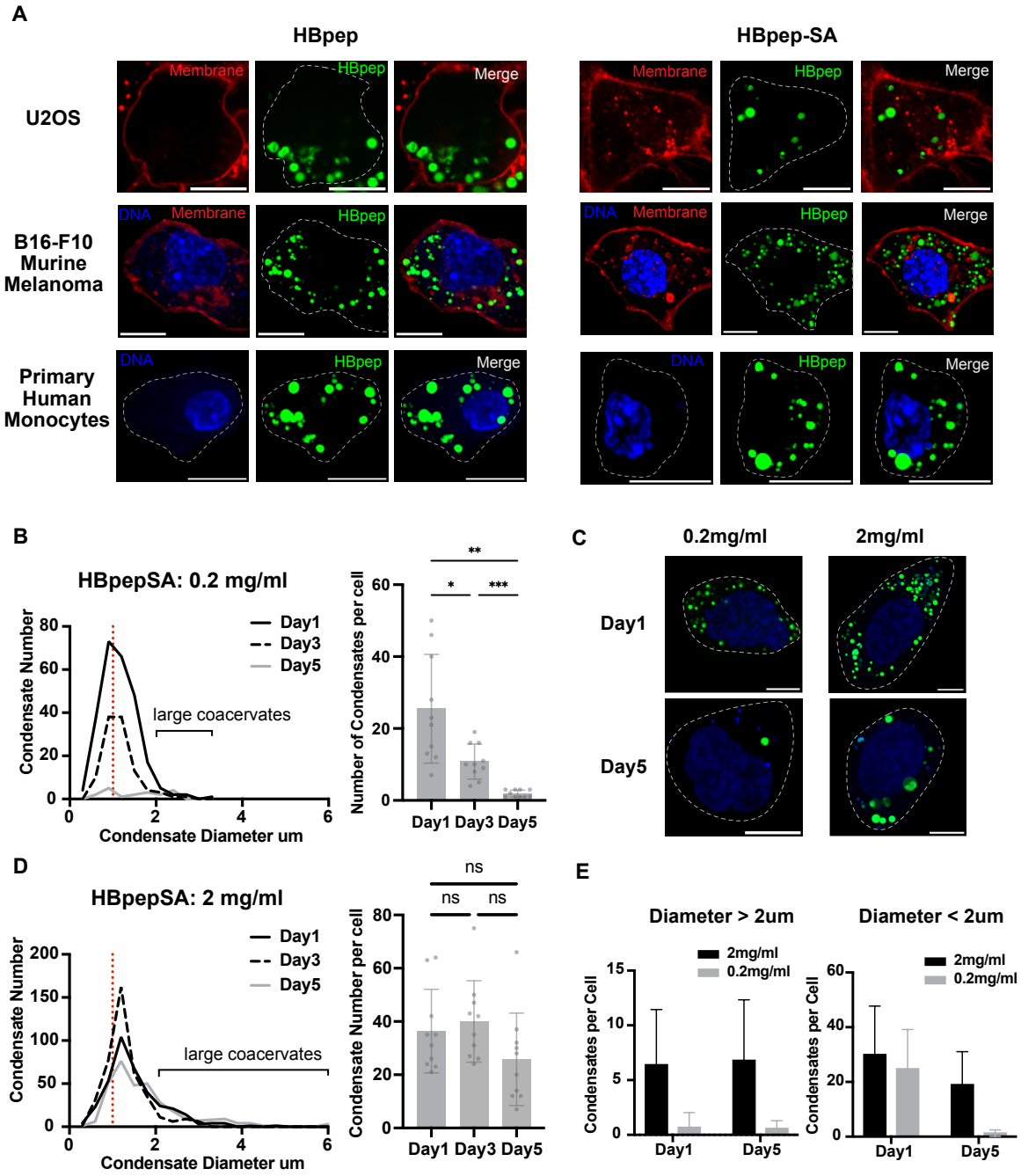

Figure 3. Stable delivery of peptide coacervates to mouse and human cells and clinically relevant cell types
(A) Fluorescence images of coacervate uptake in cell lines. 30ul of HBpep particles assembled at 1mg/mL or 30ul HBpep-SA particles assembled at 0.5mg/mL were added to the cell media for human osteosarcoma line U2OS, B16-F10 murine melanoma cells, and primary human monocytes. Green: FITC labeled condensates. Red: Abcam Cytopainter Cell Membrane Staining. Blue: Nucleus, stained DNA (DAPI). Scale bar: 10 µm. **(B)(D)** Quantification of size and number of coacervate taken up per cells; for formulations of 20 µl 0.2 mg/mL or 10ul 2 mg/mL HBpep-SA delivered to U2OS; following particles over the course of 5 days. For coacervate size quantification, n=255, 108, 19 for 0.2mg/mL from Day1 to Day5 and n= 364, 400, 353 for 2mg/mL from Day1 to Day5. For coacervate number per cell quantification, cell number n=10. Error bars indicate standard deviation. **(C)** Fluorescence images of U2OS cells with particles at day 1 and day 5. Scale bar: 10 µm. **(E)** Quantification of the number of large coacervates (diameter > 2 µm) per cell compared to smaller ones (diameter < 2 µm) for particles assembled at 2 mg/mL and 0.2 mg/mL HBpep-SA. The number of cells used for quantification per group, n=10. Error bars indicate the standard deviation. NS indicates not significant ($P > 0.05$), *$P \leq 0.05$, **$P \leq 0.01$, ***$P \leq 0.001$ and ****$P \leq 0.0001$.

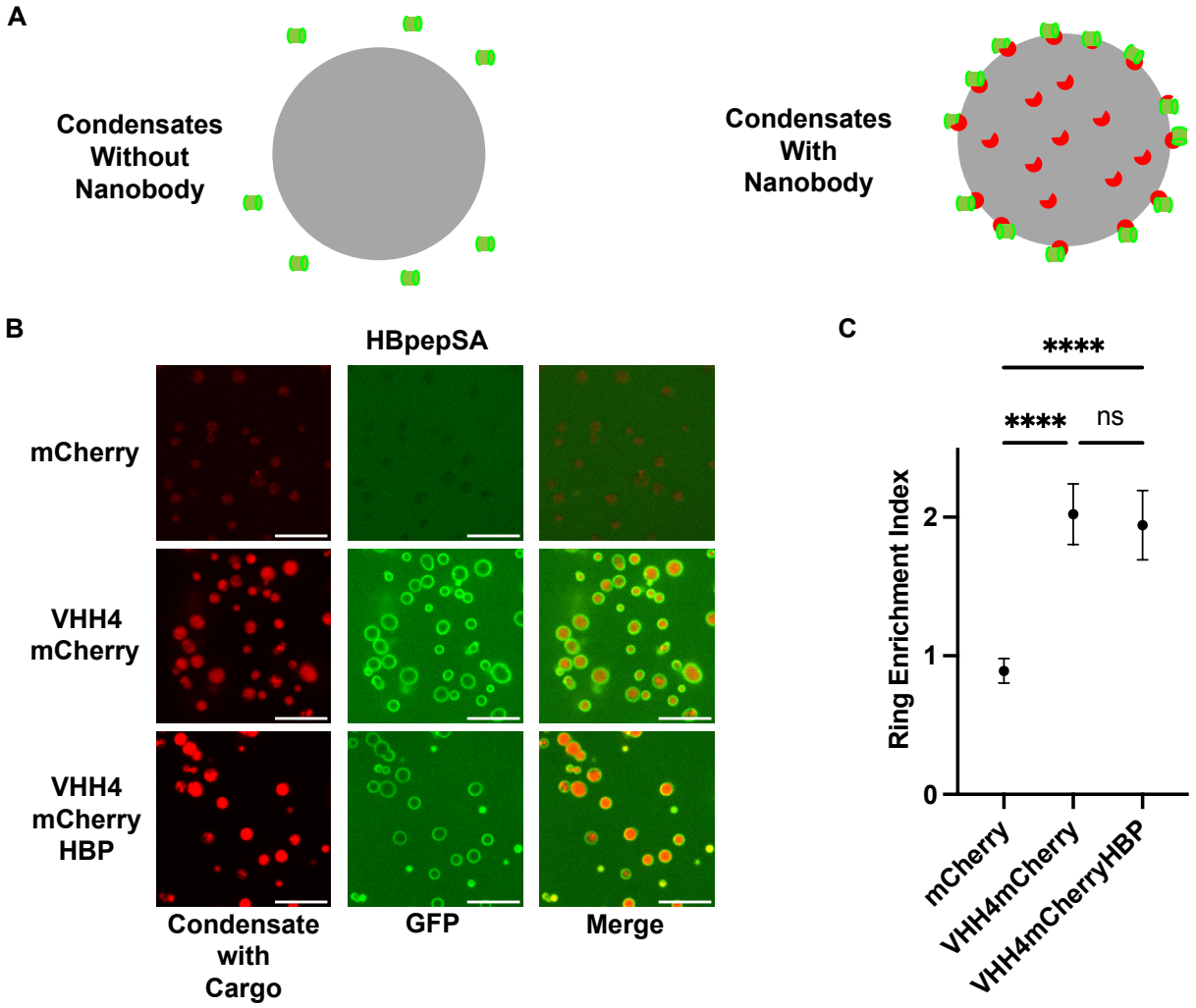

Figure 4. Selective binding of protein targets to nanobody containing coacervates in vitro
(A) Scheme to determine selectivity of target binding to mCherry loaded or VHH4-mCherry loaded HBpep coacervates. VHH4 nanobody binds GFP. **(B)** Fluorescence images of cargo (mCherry or VHH4 mCherry) and target protein (GFP) added following addition of 1uM target protein. Images taken 5mins after GFP added. scale bar: 10 µm. **(C)** Quantification of the enrichment of target GFP to HBpep-SA coacervates. enrichment index: intensity of fluorescence on particle surface division by surrounding solution. The number of condensates used for quantification per group: n=20. The error bars indicate standard deviation. NS indicates not significant ($P > 0.05$), *$P \leq 0.05$, **$P \leq 0.01$, ***$P \leq 0.001$ and ****$P \leq 0.0001$.

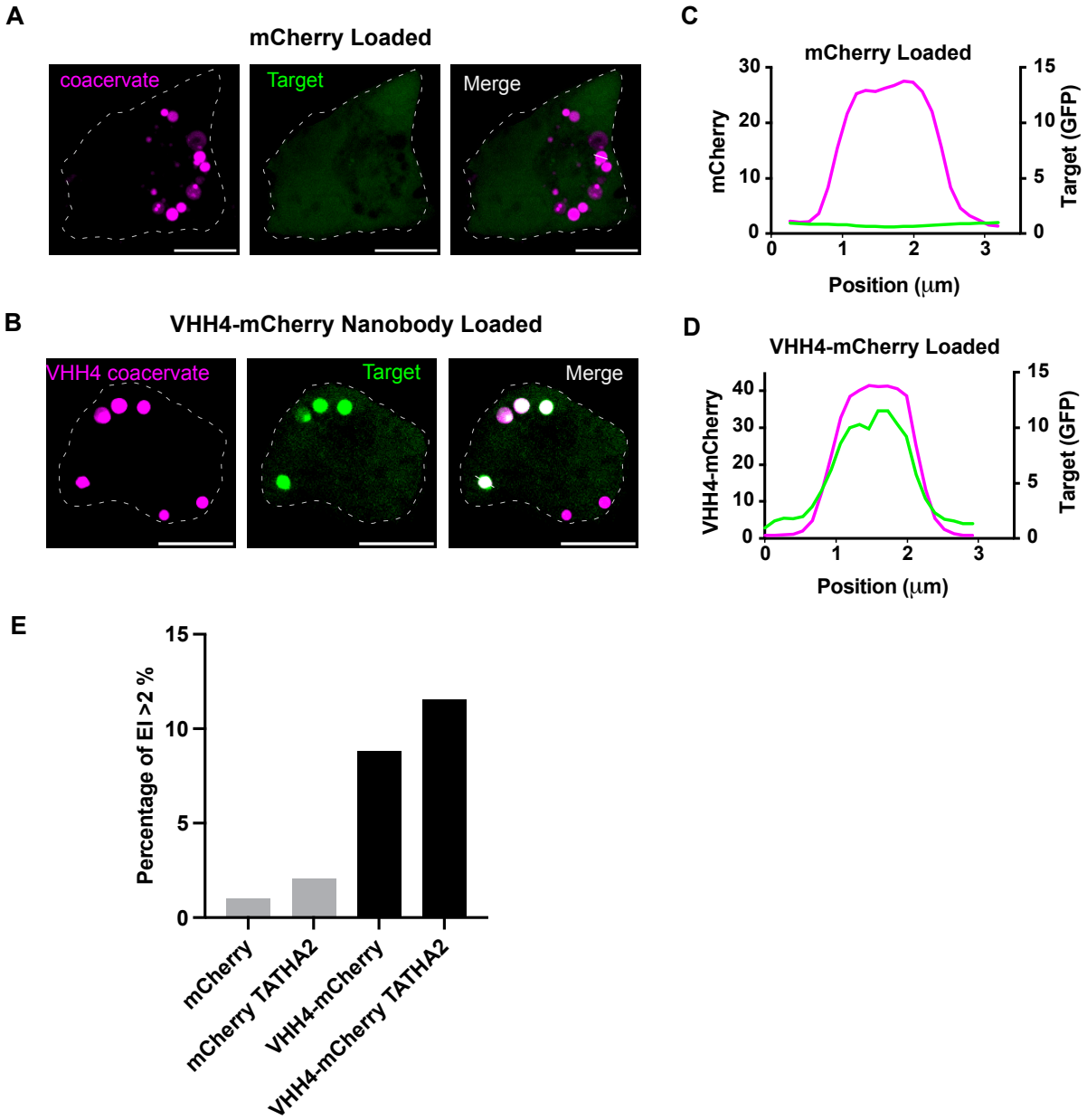

Figure 5. Delivered VHH4-HBpep-SA "Hubs" bind to and enrich native target GFP protein
(A)(B) Representative fluorescence images of target binding to hubs inside U2OS cells stably expressing GFP, comparing mCherry control and VHH4(nanobody)mCherry-loaded coacervates. 30ul of coacervates formed from 0.5 mg/mL HBpep-SA, co-assembled with 0.1mg/mL mCherry or VHH4-mCherry were added to the cell media for U2OS cells and imaged at 24 hr. Cell boundaries are indicated by dashed gray line. Chosen 'hub' for line scan is indicated by white line. Scale bar: 10 μm. **(C)(D)** Line scans of coacervate hubs showing fluorescence enrichment in (A)(B). **(E)** Quantification: percentage of hubs that show target enrichment greater than 2.